Engineering Science and Technology, an International Journal 22 (2019) 862–868

HOSTED BY

Contents lists available at ScienceDirect

Engineering Science and Technology, an International Journal

journal homepage: www.elsevier.com/locate/jestch

Full Length Article

Design and equivalent circuit model extraction of a third-order band-pass frequency selective surface filter for terahertz applications

Hamed Mohammadi Nemat-Abad *, Ehsan Zareian-Jahromi *, Raheleh Basiri

Department of Electrical Engineering, Shiraz University of Technology, Shiraz, Iran

ARTICLE INFO

Article history:
Received 7 October 2018
Revised 15 December 2018
Accepted 17 January 2019
Available online 31 January 2019

Keywords:
Equivalent circuit model
Frequency selective surface
Metamaterial
Miniaturized elements
Terahertz filter

ABSTRACT

In this paper, a third-order band-pass frequency selective surface (FSS) filter is proposed for terahertz applications. The presented FSS filter is designed based on miniaturized unit cells and a fractional bandwidth of 72% around 0.775 THz is achieved. In addition, a high transmission magnitude is obtained with an acceptable flatness in comparison to previous reports. In order to verify the numerical results, an equivalent circuit model of the proposed spatial filter is introduced considering both normal and oblique incident angles. The sensitivity of the filter with respect to the incident wave angle is investigated in the range of 0–60° whereas the obtained performance is acceptable for various incident angles in the mentioned range. Moreover, the effects of altering different geometrical parameters are studied and justified based on the extracted equivalent circuit model.

1. Introduction

Terahertz technology is an important topic in telecommunication engineering. According to recent works, many innovations are presented to bridge the gap between microwave and infrared waves, resulting in terahertz devices in the frequency range of 0.1–10 THz [1,2]. These devices are demanded in many applications including broadband telecommunications [3,4], imaging [5,6], and explosive and drug detection [5,7]. Currently, many attempts are made to develop various devices in terahertz regime such as antennas [8,9], absorbers [10], sensors [11,12], and filters [13].

Filters are widely used components in any telecommunication system. Terahertz filters can be divided into different categories including micro electro-mechanical systems [14], liquid crystal [15], graphene [16], and metamaterial (MTM) [17] based filters. MTMs and FSS structures are artificial electromagnetic materials which are applicable in many applications due to their many features including compactness and appropriate resulting performance [18–21].

MTM and FSS filters can be categorized into different structures according to the desired performance, e.g. high-pass [22], band-stop [23], and band-pass [24]. These filters are further classified based on narrow-band [25], multi-band [26], and broadband [27] performance.

Three important design pre-assumptions are considered in the design procedure of MTM terahertz structures. First, the effective homogeneous condition must be satisfied, meaning that the structure dimensions are considered to be less than $\lambda_g/4$ where λ_g is the guided wavelength. Considering this criteria, the structure can be considered as a real material [28]. Second, the structure should be symmetrical in order to reduce the corresponding sensitivity to the radiation angle of the incident wave [29,30]. Third, it is necessary to use a special type of FSS structure called miniaturized element FSS (MEFSS). This condition provides the ability to extract an equivalent circuit model of the proposed filter structure. MEFSSs are multi-layered structures with dimensions much smaller than λ_g. Considering these conditions, symmetrical multi-layer structures including non-resonant metal elements of dimensions less than $\lambda_g/5$ are highly demanded [31].

Many spatial filters have been proposed and designed in the microwave frequency range considering the previously discussed assumptions [31–33], as well as filters in terahertz regime [34,35]. In order to investigate the performance of the structure, the extraction of the corresponding equivalent circuit model is of great importance. Ebrahimi *et al.* introduced a band-pass MEFSS filter providing 45% fractional bandwidth [36]. Moreover, the presented filter yields a maximum transmission magnitude of about 0.7 whereas the structure suffers from large dimensions and considerable thickness.

* Corresponding authors.
E-mail addresses: Ha.Mohammadi@sutech.ac.ir (H. Mohammadi Nemat-Abad), Zareian@sutech.ac.ir (E. Zareian-Jahromi), r.basiri@sutech.ac.ir (R. Basiri).

Peer review under responsibility of Karabuk University.

https://doi.org/10.1016/j.jestch.2019.01.008
2215-0986/

In this paper, a band-pass MEFSS filter with third-order frequency response in terahertz regime is designed. The filter structure is innovative providing an acceptable performance for many applications. The filter provides appropriate transmission amplitude in the in-band region together with suitable filtering performance in the out-of-band region. In addition, the radiation angle sensitivity of the filter structure is low. The filter consists of three well-designed layers with first order frequency response resulting in a third-order band-pass filter structure. The equivalent circuit model is also extracted for the filter structure considering both normal and oblique incident angles. It is demonstrated that the extracted equivalent circuit schematic is general for various incidences. However, slight differences between values of lumped elements are identified for different incidences. The validity of proposed circuit model is examined whereas the corresponding results closely match the simulation ones.

The manuscript is organized as follows. The design procedure of the filter is presented in Section II. In Section III, the corresponding equivalent circuit of the MEFSS filter is discussed. The simulation results are investigated in Section IV where the structure is studied and compared to previous works. Finally, the paper is concluded in Section V.

2. Design procedure of the proposed filter

The three-dimensional geometry of the third-order MEFSS unit cell is demonstrated in Fig. 1a. The structure consists of gold layers with a thickness of t, which are separated by dielectric layers with a thickness of h_2. Additionally, two dielectric layers with a thickness of h_1 are located on top and bottom of the corresponding structure to satisfy the fabrication considerations. The middle layer is composed of a metallic ring in which a square patch with an embedded clover-shaped resonator is centrally located (Fig. 1b). The clover-shaped resonator is composed of four intersecting circles with radius r_2 which are subtracted from a square patch. The middle layer is surrounded by two identical quasi-complimentary layers (Fig. 1c). It is worth noting that the presented unit cell is inspired by a comprehensive investigation of common structures together with utilizing optimization and parametric analysis.

As previously mentioned, a symmetrical structure with miniaturized dimensions is considered in the design procedure. The presented structure is analyzed using finite element method. The geometric parameters of the structure are detailed in Table 1.

The design procedure of the MEFSS structure which is expressed from viewpoint of four developing stages can be observed in Fig. 2. At the first step, the sole metallic ring with the clover-shaped square patch is considered. According to the corresponding results in Fig. 2, a zero transmission at low frequencies is obtained.

To improve the obtained performance, the previous layers and a quasi-complementary layer are considered at the second step. It is apparent that the number of reactive elements is increased and hence, a resonance around 0.8 THz is achieved. Two high and low cut-off frequencies can be adjusted by tuning reactive elements of both layers, which is acquired as the geometric parameters are engineered.

At the third step of the design improvement, another quasi-complementary layer is added to the second step structure result-

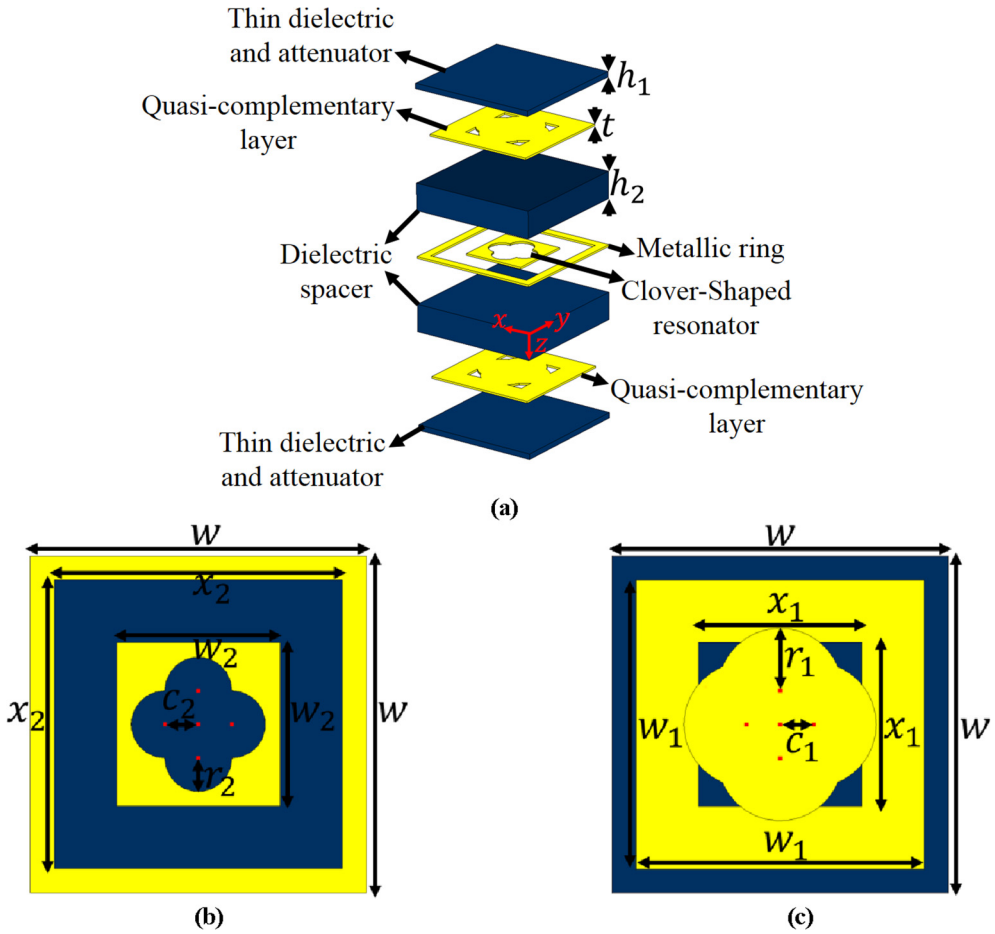

Fig. 1. (a) Expanded view of the MEFSS structure (b) middle metallic layer (c) quasi-complementary top and bottom layers.

Table 1
Geometric parameters of the presented filter in Fig. 1.

Parameters	Values (μm)	Parameters	Values (μm)
c_1	7	r_1	13
c_2	7	r_2	7
h_1	3	t	1
h_2	15	w	70
x_1	34	w_1	60
x_2	60	w_2	34

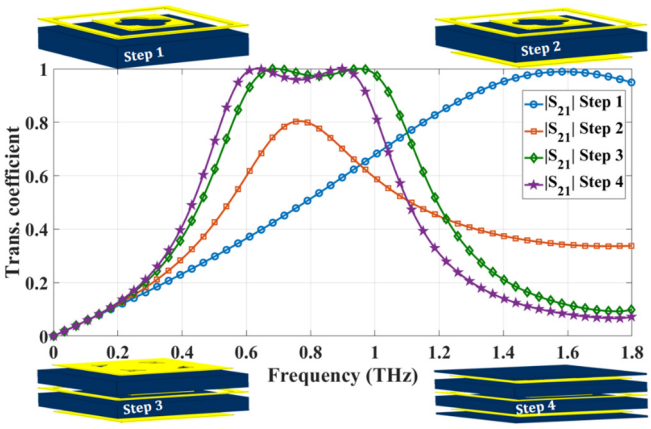

Fig. 2. Simulated step by step transmission spectra of the structure in Fig. 1 considering geometric parameters according to Table 1.

ing in an enhanced flat pass-band together with the central frequency of about 0.8 THz. The resulting flatness of the pass-band transmission spectrum can be justified according to the vicinity of resonant frequencies of the added layers.

At the final step of design procedure, the third step structure is sandwiched between two dielectric layers. Although the transmission bandwidth is slightly decreased, the structure approaches the practical counterparts [31]. It should be noted that the main role of these two dielectric layers is to protect gold on surrounding surfaces.

The structure is illuminated by an x-polarized plane wave radiating along z direction using a proper definition of Floquet port. The designed MTM filter is periodic toward x and y directions with periodicity of P. Therefore, periodic boundary condition (PBC) is considered in simulations. Fig. 3 shows the simulation procedure details of the MEFSS structure. It is worth noting that all 3D simulations are accomplished with computer simulation technology (CST) software. Moreover, the embedded frequency domain solver is utilized due its feasibility for oblique incidence simulations in comparison to time domain solver.

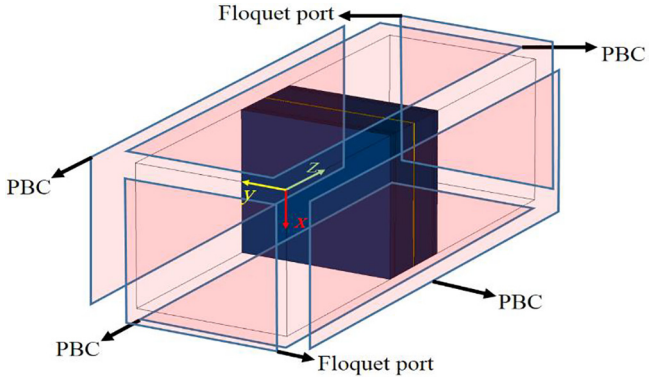

Fig. 3. Simulation details of the proposed unit cell shown in Fig. 1a.

The electric conductivity and surface impedance of lossy gold are $4.1 \times 10^7 \mathrm{S/m}$ and $0.2 + j0.22\Omega/square$, respectively. Polydimethylsiloxane (PDMS) is considered as a dielectric spacer due to its low dielectric constant ($\varepsilon_r = 2.35$) resulting in a low impedance mismatch with free space [31]. Polymeric dielectrics have minor amounts of losses and hence, can be considered as lossless materials [37].

3. Equivalent circuit model

An unmodified equivalent circuit corresponding to the MEFSS filter is shown in Fig. 4a. According to the integrity of the quasi-complementary layers, capacitors C_1 can be utilized as the corresponding equivalent circuit elements. As it is shown in Fig. 4a, the inductor L_1 represents the metallic ring inductance whereas the capacitor C_2 indicates the capacitance between the metallic ring and the clover-shaped resonator patch of the middle layer. The clover-shaped resonator is also modelled by parallel elements L_2 and C_3. Since the values of L_2 and C_3 are much lower than L_1 and C_2, the corresponding total impedance of L_2 and C_3 is negligible in comparison to that of L_1 and C_2. Therefore, the effects of L_2 and C_3 can be ignored using a proper short circuit replacement in Fig. 4b. It is also possible to consider the series resistors to the inductors to model the attenuation of the metallic layers. As it is illustrated in Fig. 4a, resistors R_1 and R_2 are placed in the equivalent circuit to calculate the mentioned attenuation.

In order to simplify the equivalent circuit, it is common to ignore the effect of the metallic layer attenuation. Based on the telegraphy transmission line model, the dielectric sections in the structure are modelled as transmission lines with characteristic impedances of $Z_{Ti} = Z_0/\sqrt{\varepsilon_{ri}}$ for $i = 1,2$ while $Z_0 = 377\Omega$ is the free space impedance and ε_{ri} is the corresponding dielectric constant. It is noted that the length of the transmission line is proportional to the height of the dielectric layers in Fig. 4b [31]. According to the extracted equivalent elements and simplifications, the MEFSS filter can be modelled as the circuit depicted in Fig. 4c.

Now, a proper method for extracting the initial values of the circuit elements in Fig. 4c is discussed as follows [27,36]:

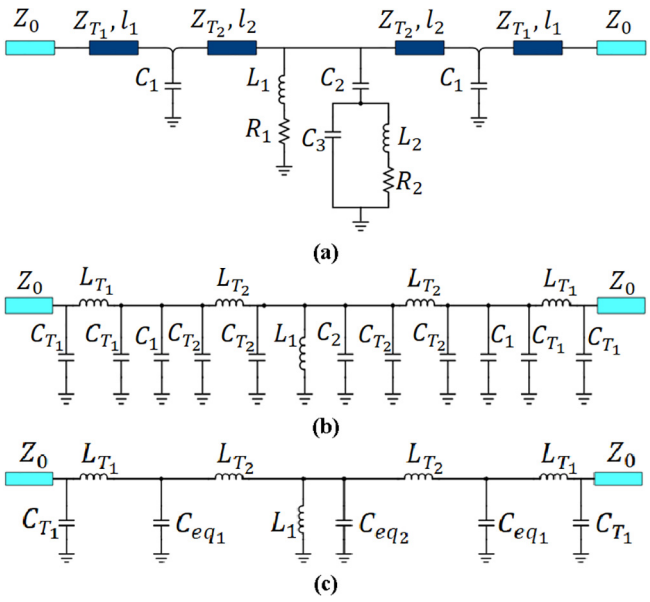

Fig. 4. (a) Unmodified equivalent circuit (b) telegraphy line approximated model (c) final equivalent circuit of the MEFSS filter in Fig. 1a.

First, the value of Ceq_1 is calculated from Eq. (1):

$$Ceq_1 = \frac{q}{2\pi f_0 r Z_0 \delta} \tag{1}$$

where q is the normalized value of the quality factors corresponding to the input and output resonators. Also, r is the normalized value of the source and load impedances. The parameter $\delta = BW/f_0$ is the fractional bandwidth where BW and f_0 are the operational bandwidth and the central frequency of the desired filter, respectively [27].

Heretofore, the value of Ceq_1 has been determined. Now, the capacitance Ceq_2 can be obtained using a tuning procedure considering an upper limit defined by:

$$Ceq_2 < \left(\frac{\sqrt{Ceq_1}}{\delta k_{1,2}}\right)^2 \tag{2}$$

where $k_{i,j}$ represents the normalized coupling coefficient between i and j substrate layers. Capacitor C_{T_1} can be determined using the equivalent circuit of transmission line model of dielectric sections as follows:

$$C_{T_1} = \frac{\varepsilon_0 \varepsilon_r h_1}{2} \tag{3}$$

where ε_0 and ε_r are the permittivity of free space and dielectric layers, respectively.

The value of L_1 can be calculated from the following equation:

$$L_1 = \frac{1}{(2\pi f_0)^2 (C_{eq1} - k_{2,3}\delta\sqrt{C_{eq1}C_{eq2}})} \tag{4}$$

The corresponding values of k, q, and r are detailed in Table 2 [36]. Finally, the coupling inductance of the successive stages can be obtained as follows:

$$L_{T_i} = \mu_0 \mu_r h_i,\ i = 1, 2 \tag{5}$$

where μ_0 and μ_r are the permeability of free space and dielectric layers, respectively.

So far, the initial values of equivalent circuit elements are specified using Eqs. (1)–(5). To obtain the final values of equivalent circuit elements, the equivalent circuit model is implemented in advance design system (ADS) software and an effective optimization algorithm with a proper goal function is utilized. The corresponding final values are obtained using a genetic optimization algorithm, an appropriate choice of target function, and consideration of simulation response limitations. The extracted schematic of equivalent circuit in Fig. 4 is consistent for both normal and oblique incident angles. Table 3 describes the corresponding optimized values of the equivalent circuit elements in Fig. 4c considering normal incidence.

4. Results and discussion

The reflection and transmission coefficients together with reflectance and transmittance ($|S_{11}|^2$ and $|S_{21}|^2$) of the MEFSS filter are shown in Fig. 5. The filter offers a relative bandwidth of 72% (0.5–1.05 THz) with an almost flat transmission performance.

Table 3
Equivalent circuit parameters in Fig. 4c considering normal incidence.

Parameters	Values (fF)	Parameters	Values (pH)
C_{T1}	2	L_{T1}	2
C_{eq1}	13.1	L_{T2}	1.9
C_{eq2}	1.6	L_1	1.5

Moreover, the maximum value of reflection coefficient ($|S_{11}|$) is less than 0.3 in 0.5–1.05 THz. Additionally, the benefit of good out-of-band rejection (less than 0.1) is achieved whereas the corresponding reflection coefficient reaches the maximum. It is noted that the proposed filter is applicable for spectroscopy and imaging applications. Also, the corresponding group delay is in order of picoseconds demonstrating a good performance for spatial filters in terahertz regime [38].

The validity of the equivalent circuit model is examined where corresponding results are compared with simulation results. The equivalent circuit results are in close accordance with full-wave simulations, revealing that different sections of the designed structure are appropriately modelled using circuit elements (Fig. 6). The values of equivalent circuit model elements are altered considering different incident angles. After using the mentioned procedure in Section 3, the related values are obtained considering oblique incident angle of 60° (Table 4). Moreover, the accuracy of these obtained values is investigated whereas corresponding results are compared with simulations (Fig. 7).

It is expected to achieve an almost insensitive structure to the angle (φ) of incident wave due to the approximately symmetric design of the designed unit cell. Therefore, the MEFSS unit cell is illuminated by incident waves with different values of φ in range of 0–60°, Fig. 8. It can be observed that the frequency peaks of the transmission spectra is almost unchanged, while the corresponding flatness is partially deteriorated for different values of φ. In the worst case of φ = 60°, the minimum value of the pass-band transmission coefficient reaches to 0.7 which is acceptable in many applications.

The geometric parameters are of great importance in the proposed MEFSS. Sweeping these parameters can provide a great insight into the general behaviour of the structure. The geometric parameters h_2 and x_2 are altered and corresponding full-wave results are demonstrated in Figs. 9 and 10. The corresponding results in the case of h_2 variations are depicted in Fig. 9. The bandwidth of the filter is proportional to the resonant frequency as [39]:

$$BW = \frac{f_c}{q} \tag{6}$$

where f_c and q are resonant frequency and the quality factor of the structure, respectively. Moreover, the resonant frequency is inversely proportional to the capacitance as follows [39]:

$$f_c = \frac{1}{2\pi\sqrt{LC}} \tag{7}$$

where L and C are corresponding inductance and capacitance values, respectively.

Table 2
Quality factor, coupling coefficients, and normalized impedance for different types of third-order filters [36].

Filter Type	q	k_{12}	k_{23}	r
Butterworth	1.000	0.7071	0.7071	1
Chebyshev (0.01 dB)	1.1811	0.6818	0.6818	1
Chebyshev (0.1 dB)	1.4328	0.6618	0.6618	1
Chebyshev (0.5 dB)	1.8636	0.6474	0.6474	1

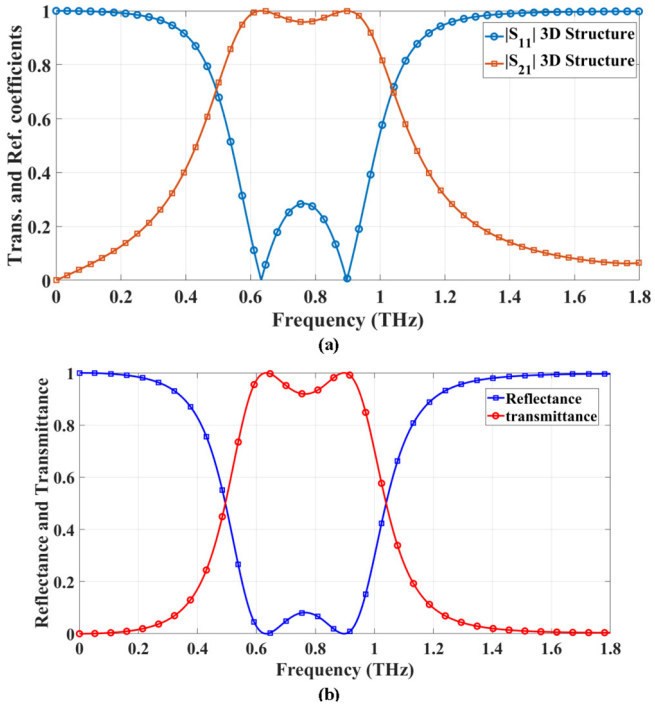

Fig. 5. Simulated results of the MEFSS structure considering the geometric parameters in Table 1(a) reflection and transmission coefficients (b) reflectance and transmittance.

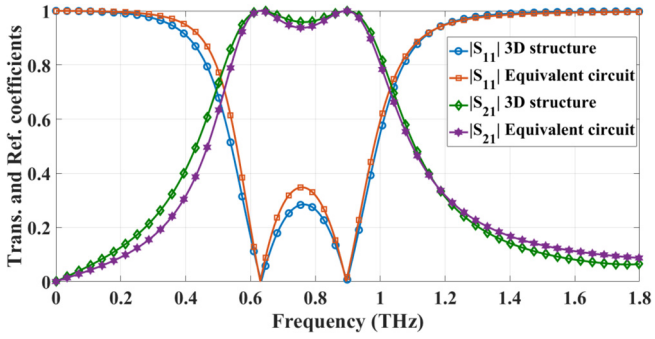

Fig. 6. Reflection and transmission spectra of full-wave simulations and equivalent circuit model of the MEFSS considering the geometric parameters in Table 1 and normal incidence.

Table 4
Equivalent Circuit Parameters in Fig. 4c considering 60° incident angle.

Parameters	Values (fF)	Parameters	Values (pH)
C_{T1}	18	L_{T1}	0.6
C_{eq1}	1	L_{T2}	0.7
C_{eq2}	3.5	L_1	1.1

The capacitance of the dielectric layer is proportional to the corresponding thickness using $C_T = \varepsilon h/2$, in which h and ε are the thickness and the permittivity of the dielectric layer, respectively [27]. Increasing dielectric thickness will increase C_T and hence, the resulting pass-band is decreased according to Eqs. (6) and (7). This procedure can also be observed in Fig. 9. Fig. 10 demonstrates the corresponding results of the case in which x_2 is altered. The value of Ceq_2 is decreased as x_2 is increased. Therefore, increased bandwidth is achieved according to Eqs. (6) and (7) following demonstrated results in Fig. 10.

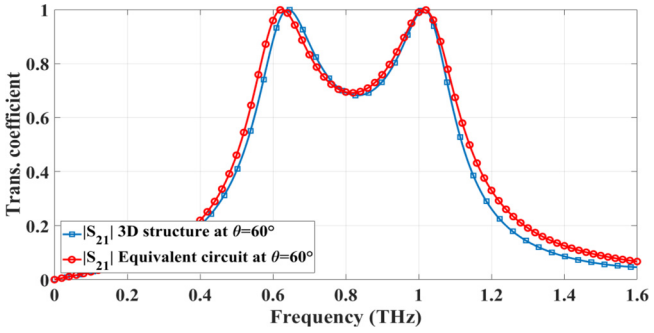

Fig. 7. Transmission spectra of full-wave simulations and equivalent circuit model of the MEFSS considering the geometric parameters in Table 1 and 60° incident angle.

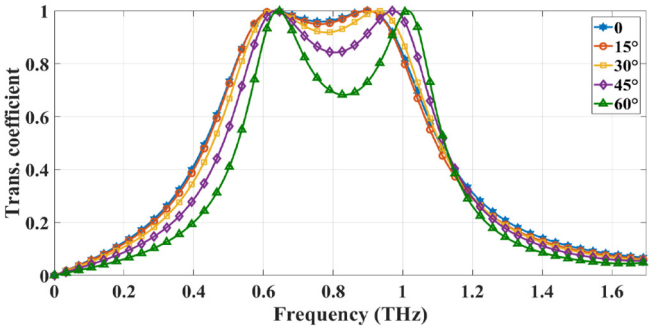

Fig. 8. Simulated transmission spectra of the MEFSS filter for different incident angles considering the geometric parameters in Table 1.

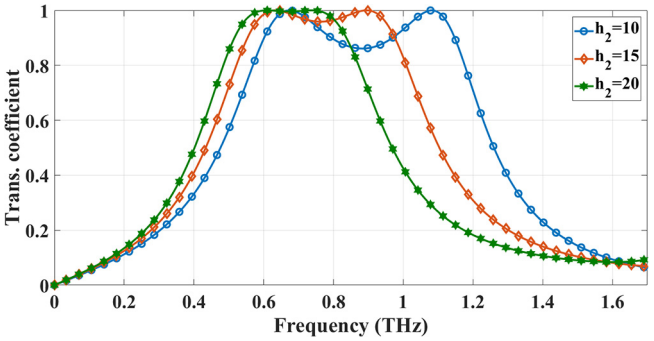

Fig. 9. Simulated transmission spectra for different values of h_2 whereas other geometric parameters are the same as mentioned in Table 1.

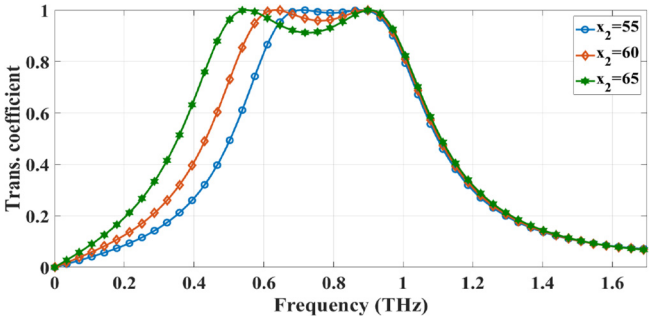

Fig. 10. Simulated transmission spectra for different values of x_2 whereas other geometric parameters are the same as mentioned in Table 1.

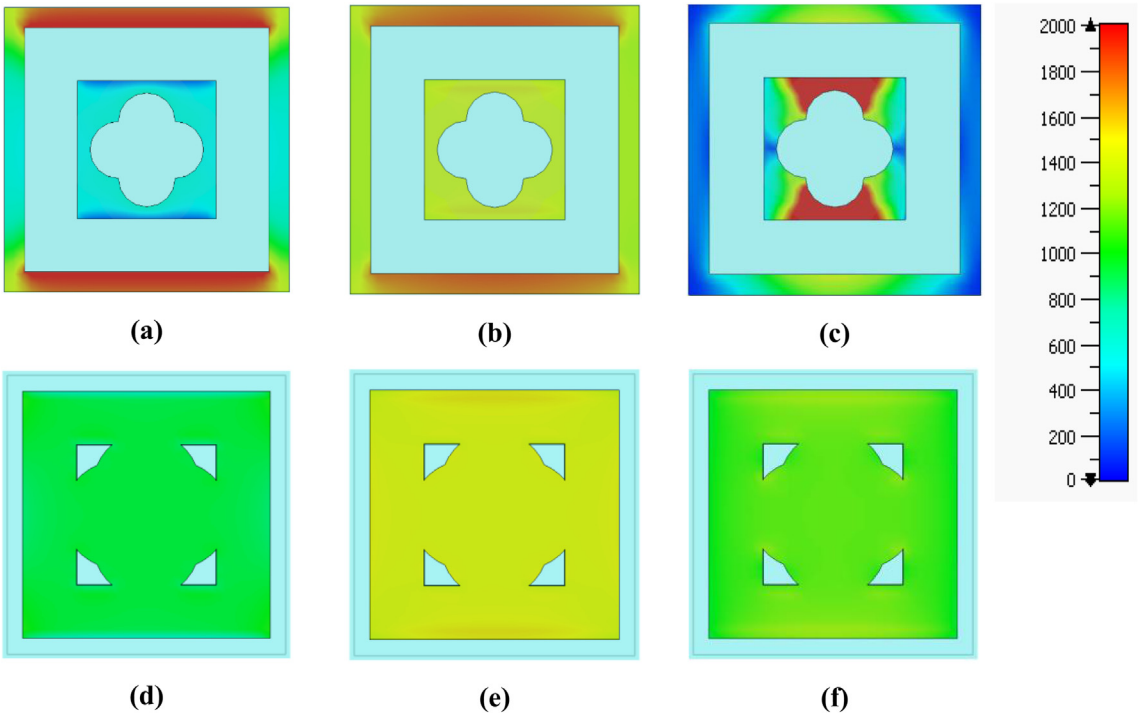

Fig. 11. Surface current distributions for different layers at various frequencies; metallic ring and clover-shaped resonator at (a) 0.2 THz, (b) 0.8 THz, (c) 1.6 THz, and quasi-complementary patch at (d) 0.2 THz, (e) 0.8 THz, (f) 1.6 THz.

Table 5
Comparison of the proposed structure and previous works.

Ref.	Bandwidth (Central Freq. THz)	Dimensions ($\mu m \times \mu m \times \mu m$)	Insertion Loss (|.|)	Pass-Band Refl. (|.|)
[31]	45% (0.42)	130 × 130 × 123	0.2	Under 0.4
[32]	44% (1.05)	210 × 210 × 130	0.1	_
[17]	22% (0.25)	90 × 90 × 230	0.15	Under 0.6
[40]	40% (1.25)	95 × 95 × 43	0.3	_
[41]	22% (0.95)	300 × 300 × 120	0.05	Under 0.3
Prop. Str.	72% (0.775)	70 × 70 × 39	0.05	Under 0.3

The surface current distributions created on metallic layers are demonstrated in Fig. 11. Three different frequencies in lower stop-band (0.2 THz), pass-band (0.8 THz), and higher stop-band (1.6 THz) are considered for more investigations. As shown in Fig. 11a and d, the major influential factor at 0.2 THz is the inductance of the metallic ring, L_1. According to Fig. 4c, a zero transmission is created by parallel L_1 at lower frequencies.

According to Fig. 11b and e, the inductance of the metallic ring, L_1, and the capacitance of the quasi-complementary patch, C_1, are mostly affecting the overall performance at 0.8 THz. Therefore, the resulting band-pass response can be justified a transmission resonance produced by a proper combination of parallel L_1 and C_1 circuit elements.

The surface current distributions in Fig. 11c and f reveal that the capacitance between metallic ring and quasi-complementary patch, C_2, plays a significant role at 1.6 THz. According to Fig. 4c, parallel C_2 results in a zero transmission at higher frequencies and hence, the corresponding higher stop-band is achieved.

A comparison of the presented structure and previous works is listed in Table 5. Obviously, the designed MEFSS is more compact and offers a broadband bandwidth. Also, it provides a proper out-of-band rejection and pass-band reflection.

5. Conclusion

In this work, a band-pass filter with small dimensions, wide pass-band, and high order of efficiency is proposed. The filter provides a fractional bandwidth of 72% around the central frequency of 0.775 THz whereas a high transmission magnitude and acceptable flatness in pass-band region are obtained. It is demonstrated that a low sensitivity to the illuminating wave angle is obtained while a great out-of-band performance is achieved. Moreover, an equivalent circuit model of the proposed filter is derived considering both normal and oblique incident angles. The validity of the extracted equivalent circuit model is demonstrated for different incident angles. The corresponding results confirm those of full-wave simulations. Also, the effects of altering geometrical parameters are investigated and justified based on the equivalent circuit model.

References

[1] J.C. Wiltse, History of millimeter and submillimeter waves, IEEE Trans. Microw. Theory Tech. 32 (1984) 1118–1127.
[2] D. Dragoman, M. Dragoman, Terahertz fields and applications, Prog. Quantum Electron. 28 (2004) 1–66.
[3] T. Kleine-Ostmann, T. Nagatsuma, A review on terahertz communications research, J. Infrared, Millimeter, Terahertz Waves 32 (2011) 143–171.
[4] J. Federici, L. Moeller, Review of terahertz and subterahertz wireless communications, J. Appl. Phys. 107 (2010) 6.
[5] K. Kawase, Y. Ogawa, Y. Watanabe, H. Inoue, Non-destructive terahertz imaging of illicit drugs using spectral fingerprints, Opt. Express 11 (2003) 2549–2554.
[6] D.M. Mittleman, M. Gupta, R. Neelamani, R.G. Baraniuk, J.V. Rudd, M. Koch, Recent advances in terahertz imaging, Appl. Phys. B 68 (1999) 1085–1094.
[7] Y.C. Shen, A.T. Lo, P.F. Taday, B.E. Cole, W.R. Tribe, M.C. Kemp, Detection and identification of explosives using terahertz pulsed spectroscopic imaging, Appl. Phys. Lett. 86 (2005) 241116.

[8] M. Dragoman, A.A. Muller, D. Dragoman, F. Coccetti, R. Plana, Terahertz antenna based on graphene, J. Appl. Phys. 107 (2010) 104313.
[9] M. Tamagnone, J.S. Gomez-Diaz, J.R. Mosig, J. Perruisseau-Carrier, Reconfigurable terahertz plasmonic antenna concept using a graphene stack, Appl. Phys. Lett. 101 (2012) 214102.
[10] H. Tao, N.I. Landy, C.M. Bingham, X. Zhang, R.D. Averitt, W.J. Padilla, A metamaterial absorber for the terahertz regime: design, fabrication and characterization, Opt. Express 16 (2008) 7181–7188.
[11] Y. Zhang, T. Li, B. Zeng, H. Zhang, H. Lv, X. Huang, W. Zhang, A.K. Azad, A graphene based tunable terahertz sensor with double Fano resonances, Nanoscale 7 (2015) 12682–12688.
[12] F. Miyamaru, S. Hayashi, C. Otani, K. Kawase, Y. Ogawa, H. Yoshida, E. Kato, Terahertz surface-wave resonant sensor with a metal hole array, Opt. Lett. 31 (2006) 1118–1120.
[13] R. Mendis, A. Nag, F. Chen, D.M. Mittleman, A tunable universal terahertz filter using artificial dielectrics based on parallel-plate waveguides, Appl. Phys. Lett. 97 (2010) 131106.
[14] Z. Han, K. Kohno, T. Makela, T. Haatainen, H. Fujita, K. Hirakawa, H. Toshiyoshi, A MEMS reconfigurable metamaterial for terahertz filter applications, in: Advanced Electromagnetic Materials in Microwaves and Optics (METAMATERIALS), 2014 8th International Congress On, IEEE, 2014, pp. 346–348.
[15] C.-Y. Chen, C.-L. Pan, C.-F. Hsieh, Y.-F. Lin, R.-P. Pan, Liquid-crystal-based terahertz tunable Lyot filter, Appl. Phys. Lett. 88 (2006) 101107.
[16] D. Correas-Serrano, J.S. Gomez-Diaz, J. Perruisseau-Carrier, A. Alvarez-Melcon, Graphene-based plasmonic tunable low-pass filters in the terahertz band, IEEE Trans. Nanotechnol. 13 (2014) 1145–1153.
[17] M. Lu, W. Li, E.R. Brown, Second-order bandpass terahertz filter achieved by multilayer complementary metamaterial structures, Opt. Lett. 36 (2011) 1071–1073.
[18] C. Caloz, T. Itoh, Electromagnetic Metamaterials: Transmission Line Theory and Microwave Applications, John Wiley & Sons, 2005.
[19] M. Gil, J. Bonache, F. Martin, Metamaterial filters: a review, Metamaterials 2 (2008) 186–197.
[20] B.A. Munk, Frequency Selective Surfaces: Theory and Design, John Wiley & Sons, 2005.
[21] E. Zareian-Jahromi, J. Khalilpour, Analysis of a freestanding frequency selective surface loaded with a nonlinear element, J. Electr. Waves Appl. 25 (2011) 247–255.
[22] H. Butt, Q. Dai, P. Farah, T. Butler, T.D. Wilkinson, J.J. Baumberg, G.A. Amaratunga, Metamaterial high pass filter based on periodic wire arrays of multiwalled carbon nanotubes, Appl. Phys. Lett. 97 (2010) 163102.
[23] X. Li, L. Yang, C. Hu, X. Luo, M. Hong, Tunable bandwidth of band-stop filter by metamaterial cell coupling in optical frequency, Opt. Express 19 (2011) 5283–5289.
[24] J.-C. Zhang, Y.-Z. Yin, J.-P. Ma, Design of narrow band-pass frequency selective surfaces for millimeter wave applications, Prog. Chem. Org. Nat. Prod. Electromagn. Res. 96 (2009) 287–298.
[25] F. Lan, Z. Yang, L. Qi, X. Gao, Z. Shi, Terahertz dual-resonance bandpass filter using bilayer reformative complementary metamaterial structures, Opt. Lett. 39 (2014) 1709–1712.
[26] N.R. Han, Z.C. Chen, C.S. Lim, B. Ng, M.H. Hong, Broadband multi-layer terahertz metamaterials fabrication and characterization on flexible substrates, Opt. Express 19 (2011) 6990–6998.
[27] M.A. Al-Joumayly, N. Behdad, A generalized method for synthesizing low-profile, band-pass frequency selective surfaces with non-resonant constituting elements, IEEE Trans. Antennas Propag. 58 (2010) 4033–4041.
[28] K. Sarabandi, N. Behdad, A frequency selective surface with miniaturized elements, IEEE Trans. Antennas Propag. 55 (2007) 1239–1245.
[29] M. Salehi, N. Behdad, A second-order dual X-/Ka-band frequency selective surface, IEEE Microwave Wirel. Compon. Lett. 18 (2008) 785–787.
[30] X.-D. Hu, X.-L. Zhou, L.-S. Wu, L. Zhou, W.-Y. Yin, A miniaturized dual-band frequency selective surface (FSS) with closed loop and its complementary pattern, IEEE Antennas Wirel. Propag. Lett. 8 (2009) 1374–1377.
[31] A. Ebrahimi, S. Nirantar, W. Withayachumnankul, M. Bhaskaran, S. Sriram, S.F. Al-Sarawi, D. Abbott, Second-order terahertz bandpass frequency selective surface with miniaturized elements, IEEE Trans. Terahertz Sci. Technol. 5 (2015) 761–769.
[32] J.-S. Li, Y. Li, L. Zhang, Terahertz bandpass filter based on frequency selective surface, IEEE Photonics Technol. Lett. 30 (2018) 238–241.
[33] Y. Zhu, S. Vegesna, V. Kuryatkov, M. Holtz, M. Saed, A.A. Bernussi, Terahertz bandpass filters using double-stacked metamaterial layers, Opt. Lett. 37 (2012) 296–298.
[34] S. Das, K.M. Reza, M.A. Habib, Frequency selective surface based bandpass filter for THz communication system, J. Infrared, Millimeter, Terahertz Waves 33 (2012) 1163–1169.
[35] D.M. Pozar, Microwave Engineering, John Wiley & Sons, 2009.
[36] A.I. Zverev, Handbook of Filter Synthesis, Wiley, 1967.
[37] A. Podzorov, G. Gallot, Low-loss polymers for terahertz applications, Appl. Opt. 47 (2008) 3254–3257.
[38] C. Winnewisser, F. Lewen, H. Helm, Transmission characteristics of dichroic filters measured by THz time-domain spectroscopy, Appl. Phys. A Mater. Sci. Process. 66 (1998) 593–598.
[39] R.F. Harrington, Time-harmonic Electromagnetic Fields, McGraw-Hill, 1961.
[40] Y.-J. Chiang, C.-S. Yang, Y.-H. Yang, C.-L. Pan, T.-J. Yen, An ultrabroad terahertz bandpass filter based on multiple-resonance excitation of a composite metamaterial, Appl. Phys. Lett. 99 (2011) 191909.
[41] X. Ri-Hui, L. Jiu-Sheng, Double-layer frequency selective surface for terahertz bandpass filter, J. Infrared, Millimeter, Terahertz Waves (2018) 1–8.